Mathematical Analysis of Carreau Fluid model for Blood Flow in Tapered Constricted Arteries

D. S. Sankar[1], Usik Lee[2], Atulya K. Nagar[3], Maziri bin Dr. Hj Morsidi[4]

[1]Engieering Mathematics Unit, Faculty of Engineering, Universiti Teknologi Brunei, Jalan Tungku Link, BE1410, Gadong, Brunei Darussalam
[2]Department of Mechanical Engineering, Inha University, Inha-Ro 100, 253 Yonghyun-Dong, Nam-Gu, Incheon 402-751, Republic of Korea
[3]Department of Mathematics and Computer Science, Centre for Applicable Mathematics and Systems Science, Liverpool Hope University, Hope Park, Liverpool L16 9JD, UK
[4]Department of Mechanical Engineering, Faculty of Engineering, Universiti Teknologi Brunei, Jalan Tungku Link, Gadong, BE 1410, Brunei Darussalam

{duraisamy.sankar@utb.edu.bn, ulee@inha.ac.kr, nagara@hope.ac.uk, maziri.morsidi@utb.edu.bn}

Abstract: The pulsatile flow of blood through a tapered constricted narrow artery is investigated in this study, treating the blood as Carreau fluid model. The constriction in the artery is due to the formation of asymmetric stenosis in the lumen of the artery. The expressions obtained by Sankar (2016) for the various flow quantities are used to analyze the flow with different arterial geometry. The influence of various flow parameters on the velocity distribution, wall shear stress and longitudinal impedance to flow is discussed. The velocity of blood increases with the increase of the power law index and stenosis shape parameter and it decreases considerably with the increase of the maximum depth of the stenosis. The wall shear stress and longitudinal impedance to flow decrease with the increase stenosis shape parameter, amplitude of the pulsatile pressure gradient, flow rate, power law index and Weissenberg number. The estimates of the percentage of increase in the wall shear stress and longitudinal impedance to flow increase with the increase of the angle tapering and these increase significantly with the increase of the maximum depth of the stenosis. The mean velocity of blood decreases considerably with the increase of the artery radius (except in arteriole), maximum depth of the stenosis and angle of tapering and it is considerably higher in pulsatile flow of blood than in the steady flow of blood.

***Keywords*:** Mathematical model, Perturbation analysis, Pulsatile Blood flow, Carreau fluid, Asymmetric stenosis, Mean velocity.

1. Introduction

Arteries are constricted due to the development of stenosis in the lumen of the arteries by the deposit of fatty substances such as lipids, cholesterol etc [1]. Stenosis growth passes through three stages. In the first stage, the stenosis is mild and the flow is laminar, there is no flow separation and no back flow occurs. In stage II, the stenosis is moderate in size and the flow is still laminar, but, there is flow separation and back flow occurs. In stage III, the stenosis size is significant and turbulent flow develops in the central region downstream [2 - 4]. In the lumen of the blood vessels, stenoses are formed naturally in different shapes like axi-symmetric, asymmetric, multiple, overlapping etc [5 - 6]. The shape and size of stenosis are the prime parameters which significantly changes the blood flow characteristics. Once a stenosis develops in the lumen of an artery, it alters the flow field, changes the pressure distribution, reduces the velocity of blood and increases the resistance to flow. Tang and Yang [7] propounded that the stenosed arteries collapse due to low blood pressure around the stenotic portion. Consequently, stenosis development in the blood vessels leads to serious cardiovascular diseases like, heart attack, ischemia strokes like cardiac ischemia, brain ischemia etc [8]. Hence, it is important to study the fluid dynamics of blood flow in stenosed arteries.

Several researchers attempted to study the effects of stenosis size and shape on the blood flow characteristics, treating the blood as Newtonian fluid which is found to be valid only when it flows through arteries of larger diameters ($>1300\,\mu m$) at high shear rates ($>100\,s^{-1}$) [9, 10]. Since, blood exhibits significant non-Newtonian flow characteristics when it flows in small diameter arteries (artery diameter $50\mu m$–$1300\mu m$) at low shear rates ($<100\,s^{-1}$), several researchers attempted to investigate the effect of non-Newtonian character blood on the physiologically important flow quantities such as skin friction and impedance to flow under normal and abnormal (stenosis, aneurysm, catheter, stenting etc) flow conditions [11, 12]. It is well accepted that blood flow in arteries is highly pulsatile, particularly when it flows in narrow arteries with stenosis [13].

To predict the flow characteristics of blood through the use of suitable fluid model, Cho and Kensey [14] analyzed several non-Newtonian fluid models including Power law and Carreau fluid models and compared their results with the experimental results of others. Johnson et al. [15] propounded that the Carreau fluid model is a generalized Newtonian fluid model which is most appropriate for modeling blood when it flows through narrow arteries at low shear rates. They also reported that the Carreau fluid model does not over predict the fluid behavior near the arterial wall when the blood viscosity is high with a significant non-Newtonian influence on the flow. Chang et al [16] observed that Carreau fluid model has the high flexibility that it could be used to model blood when it flows through both larger diameter and smaller diameter arteries. Since, Carreau fluid

model's constitutive equation has four physical parameters, one can obtain more detailed information on the flow characteristics of blood in a wide range of shear rates [17]. Carreau fluid model's constitutive equation can be reduced to represent Newtonian fluid behavior when the power law index is unity or the time constant is zero or both. Hence, in view of the aforementioned arguments, it is more appropriate to model the blood as Carreau fluid when it flows through narrow diameter arteries.

Johnston et al. [15] used several non-Newtonian fluid models including Carreau fluid model in their investigate on the wall shear stress distribution in blood flow through stenostic arteries and pointed out that Carreau fluid model is the best among all the other fluid models, since it showed very good agreement with their experimental data. Chang et al [16] numerically analyzed the fluid-solid structure interaction between blood and arterial wall and found that the wall shear stress is highest at the throat of the stenosis. Akbar [17] studied the effects of heat and mass transfer in blood flow through a tapered stenotic artery, modeling blood as Carreau fluid model. Akbar and Nadeem [18] investigated the steady flow of blood in a tapered artery with mild stenosis, treating blood as Carreau fluid model and used perturbation method to obtain the asymptotic solutions.Sankar [19] mathematically analyzed the pulsatile flow of blood in a tapered artery with overlapping stenosis, treating blood as Carreau fluid model.

As the stenoses are formed in the lumen of the arteries in arbitrary shapes, in fact, naturally these would be asymmetric in shape and thus it is not appropriate to assume the shape of stenoses as exactly axi-symmetric. Inspired by this fact, we propose to study the pulsatile flow of blood in a tapered narrow artery with asymmetric stenosis, treating blood as Carreau fluid model. This research problem has not been studied any researcher so far, to the knowledge of the authors. The expressions obtained by Sankar [19] for the flow quantities are used to obtain data for plotting the graphs for the present study. For the independent understanding of this paper, the expressions obtained for the flow quantities by Sankar [19] are derived in this paper in very concise form.

2. Mathematical formulation

Consider the pulsatile, axially symmetric, laminar and fully developed flow of blood (assumed as viscous incompressible fluid) in the axial direction through a circular tapered narrow artery with mild overlapping constriction (stenosis). The geometry of segment of a tapered narrow artery with mild asymmetric stenosis is shown in Fig. 1a. Cylindrical polar coordinate system (r,ϕ,z) is used to analyze the flow, where r and z are the coordinates in the radial and axial directions respectively and ϕ is the azimuthal angle. The segment of a tapered stenosed artery is shown in Fig. 1a. The shapes of the tapered stenosed artery for different values of n, δ and ψ are depicted in Figure 1b. The geometry of segment of tapered stenosed artery as shown in Figure 1a is represented in non-dimensional form as below (refer Sankar [19] for dimensional form of this equation):

$$h(z)=(1+\zeta z)\left[1-\delta\left((z-\sigma)-(z-\sigma)^{n}\right)\right],\ \sigma\le z\le\sigma+1 \quad (1)$$

where $\sigma=a/b$, a is the location of the starting position of the stenosis, b is the length of the stenosis, δ is the maximum depth of the stenosis, ψ is the angle of tapering of the artery, $\zeta=\tan\psi$, n is the power law index. It is noted that when $n=2$, Eq. (1) represents the geometry of segment of artery with axi-symmetric stenosis.

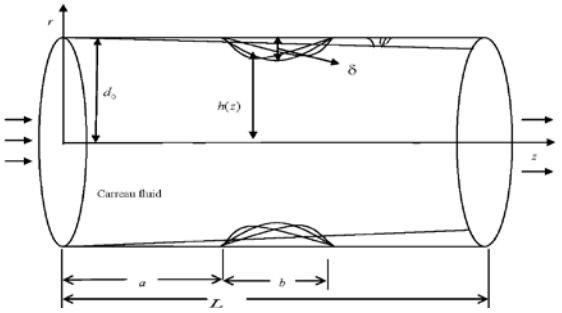

(a) Geometry of segment of tapered stenosed artery.

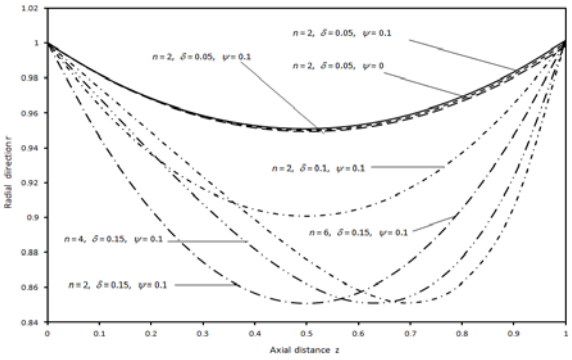

(b) Shapes of artery for different naues of n, δ and ψ.

Figure 1. Geometry of segment of a tapered stenosed artery.

The simplified non-dimensional form of axial component of the momentum equation and the constitutive equation of Carreau fluid model are given below:

$$\alpha^{2}\frac{\partial u}{\partial t}=-\frac{\partial p}{\partial z}+\frac{1}{r}\frac{\partial}{\partial r}(r\tau), \quad (2)$$

$$\tau=\left(\frac{\partial u}{\partial r}\right)+We^{2}\left(\frac{m-1}{2}\right)\left(\frac{\partial u}{\partial r}\right)^{3}. \quad (3)$$

where α is the pulsatile Reynolds number, u is the axial velocity of the fluid flow, τ is the shear stress, We is the Weissenberg number, m is the power law index, p is the fluid pressure. Using Eq. (2) in Eq. (3), one can get the simplified form of equation of motion as below:

$$\alpha^{2}\frac{\partial u}{\partial t}=-\frac{\partial p}{\partial z}+\frac{1}{r}\frac{\partial}{\partial r}\left[r\left\{\left(\frac{\partial u}{\partial r}\right)+We^{2}\left(\frac{m-1}{2}\right)\left(\frac{\partial u}{\partial r}\right)^{3}\right\}\right]. \quad (4)$$

The dimensionless form of the appropriate boundary conditions to the flow field

$$\frac{\partial u}{\partial r}=0 \ \ at\ r=0, \quad (5)$$

$$u = 0 \ \ at \ r = R. \tag{6}$$

Eq. (4) need to be solved for the fluid's velocity u subject to the boundary conditions (5) and (6).

3. Perturbation method of Solution

Let us assume the pressure gradient in the variable separable form as given below:

$$\frac{\partial p}{\partial z} = q(z)\, f(t), \tag{7}$$

where $q(z) = dp/dz = \partial p(z,0)/\partial t$ is the steady state pressure gradient and $f(t)$ is the pressure gradient in the transient state. Since the flow is assumed as pulsatile, $f(t)$ is taken as $f(t) = 1 + A\sin t$ (periodic function of time). Since, Eq. (4) is a nonlinear partial differential equation which cannot be solved by direct methods; we employ the embedded perturbation method to solve it along with the boundary conditions (5) and (6). Since we assumed the flow as slow and pulsatile, the pulsatile Reynolds number α and Weissenberg number *We* are very small, it is wise to expand the unknown flow quantities in the perturbation series about the square of these parameters. First of all, we expand the velocity u, steady state pressure gradient q and flow rate Q in the perturbation series about the square of the Weissenberg number *We* as below:

$$u(r,z,t) = u_0(r,z,t) + We^2\ u_1(r,z,t) + ..., \tag{8}$$

$$q(z) = q_0(z) + We^2\ q_1(z) + ..., \tag{9}$$

$$Q(z,t) = Q_0(z,t) + We^2\ Q_1(z,t) + ..., \tag{10}$$

Using Eqs. (8) and (9) in Eq. (4) and then simplifying, we obtain the following equations as the result of the zeroth order and first order approximations respectively:

$$\alpha^2 \frac{\partial u_0}{\partial t} = -q_0(z)\, f(t) + \frac{1}{r}\frac{\partial}{\partial r}\left[r\left(\frac{\partial u_0}{\partial r} \right) \right], \tag{11}$$

$$\alpha^2 \frac{\partial u_1}{\partial t} = -q_1(z)\, f(t) + \frac{1}{r}\frac{\partial}{\partial r}\left[r\left(\frac{\partial u_1}{\partial r} \right) \right] + \left(\frac{m-1}{2} \right)\frac{1}{r}\frac{\partial}{\partial r}\left[r\left(\frac{\partial u_0}{\partial r} \right)^3 \right]. \tag{12}$$

Substituting Eq. (8) in Eqs. (5) and (6) and then simplifying, we get the zeroth and first order approximations to the boundary conditions as

$$\frac{\partial u_0}{\partial r} = 0 \ \text{ and } \ \frac{\partial u_1}{\partial r} = 0 \ \text{ at } r = 0, \tag{13}$$

$$u_0 = 0 \text{ and } u_1 = 0 \ \text{ at } r = R. \tag{14}$$

As Eqs. (11) and (12) are not solvable directly, we expand the velocity components u_0 and u_1 in the perturbation series about the square of the pulsatile Reynolds number α as below:

$$u_0(r,z,t) = u_{00}(r,z,t) + \alpha^2 u_{01}(r,z,t) + ..., \tag{15}$$

$$u_1(r,z,t) = u_{10}(r,z,t) + \alpha^2 u_{11}(r,z,t) + ... \tag{16}$$

Using Eq. (15) in Eq. (11) and simplifying the resulting equation and then equating the zeroth order terms and first order terms, one can get the following equations respectively.

$$0 = -q_0(z)\, f(t) + \frac{1}{r}\frac{\partial}{\partial r}\left[r\left(\frac{\partial u_{00}}{\partial r} \right) \right], \tag{17}$$

$$\frac{\partial u_{00}}{\partial t} = \frac{1}{r}\frac{\partial}{\partial r}\left[r\left(\frac{\partial u_{01}}{\partial r} \right) \right]. \tag{18}$$

Applying Eqs. (15) and (16) in Eq. (12) and simplifying the resulting equation and then equating the zeroth order and first order terms, we get he following equations respectively.

$$0 = -q_1(z)\, f(t) + \frac{1}{r}\frac{\partial}{\partial r}\left[r\left(\frac{\partial u_{10}}{\partial r} \right) \right] + \left(\frac{m-1}{2} \right)\frac{1}{r}\frac{\partial}{\partial r}\left[r\left(\frac{\partial u_0}{\partial r} \right)^3 \right], \tag{19}$$

$$\frac{\partial u_{10}}{\partial t} = \frac{1}{r}\frac{\partial}{\partial r}\left[r\left(\frac{\partial u_{11}}{\partial r} \right) \right]. \tag{20}$$

Using Eqs. (15) and (16) in the boundary conditions (13) and (14), we get the zeroth and first order approximations as the following boundary conditions:

$$\frac{\partial u_{00}}{\partial r} = 0 \ \text{ and } \ \frac{\partial u_{01}}{\partial r} = 0 \ \text{ at } r = 0, \tag{21}$$

$$\frac{\partial u_{10}}{\partial r} = 0 \ \text{ and } \ \frac{\partial u_{11}}{\partial r} = 0 \ \text{ at } r = 0, \tag{22}$$

$$u_{00} = 0 \text{ and } u_{01} = 0 \ \text{ at } r = R, \tag{23}$$

$$u_{10} = 0 \text{ and } u_{11} = 0 \ \text{ at } r = R. \tag{24}$$

Solving Eqs. (17) – (18) along with the Eqs. (21) and (23), we obtain

$$u_{00} = -\frac{1}{4}\left[q_0(z)\, f(t) \right] h^2 \left[1 - (r/h)^2 \right], \tag{25}$$

$$u_{01} = \frac{1}{64}\left[q_0(z)\, f(t) \right] B h^4 \left[3 - 4(r/h)^2 + (r/h)^4 \right], \tag{26}$$

where $B = \left(1/f(t)\right)(df/dt)$. Substituting Eqs. (25) and (26) in Eq. (15), one can obtain the expression for u_0 as given below:

$$u_0 = -\frac{1}{64}\left[q_0(z)\, f(t) \right] h^2 \left[16\left\{ 1 - (r/h)^2 \right\} - B\alpha^2 h^2 \left\{ 3 - 4(r/h)^2 + (r/h)^4 \right\} \right] \quad . \tag{27}$$

Solving Eqs. (19) and (20) with the help of Eqs. (22), (24) and (27), one can obtain the following expression for u_{10} and u_{11}.

$$u_{10} = -\frac{1}{4}\left[q_1(z)\, f(t) \right] h^2 \left\{ 1 - (r/h)^2 \right\} + \left(\frac{m-1}{64} \right)\left[q_0(z)\, f(t) \right]^3 h^4 \left[\left\{ 1 - (r/h)^4 \right\} \right.$$

$$+\frac{Bh^2\alpha^2}{12}\left\{1-(r/h)^6\right\}-9\left\{1-(r/h)^4\right\}\Big] \quad (28)$$

$$u_{11}=\frac{1}{64}\left[q_1(z)\,f(t)\right]Bh^4\left\{3-4(r/h)^2+(r/h)^4\right\}$$

$$-\frac{3(m-1)}{64}\left[q_0(z)\,f(t)\right]^3Bh^6\Big[\frac{1}{36}\left\{8-9(r/h)^2+(r/h)^6\right\}$$

$$+\frac{(3B+D)\alpha^2}{12}\Big\{\frac{1}{64}\left(15-16(r/h)^2+(r/h)^8\right)$$

$$-\frac{9h^2}{36}\left(8-9(r/h)^2+(r/h)^6\right)\Big\}\Big] \quad (29)$$

where $D=(1/B)(dB/dt)$. Using Eqs. (28) and (29) in Eq. (16) and then neglecting the terms involving α^4 and higher powers of α, one can get the simplified form of the expression for u_1 as below:

$$u_1=-\frac{\left[q_1(z)\,f(t)\right]h^2}{4}\left\{1-(r/h)^2\right\}$$

$$+\frac{\alpha^2\left[q_1(z)\,f(t)\right]Bh^4}{64}\left\{3-4(r/h)^2+(r/h)^4\right\}$$

$$+\frac{(m-1)\left[q_0(z)\,f(t)\right]^3h^4}{64}\left\{1-(r/h)^4\right\}$$

$$-\frac{(m-1)B\alpha^2h^6\left[q_0(z)\,f(t)\right]^3}{768}$$

$$\left\{16-9(r/h)^2-9(r/h)^4+2(r/h)^6\right\} \quad (30)$$

Using Eq. (27), one can obtain the zeroth approximation to the volume flow rate as below:

$$Q_0=\int_0^h u_0\,r\,dr=-\frac{h^4}{96}\left[q_0(z)\,f(t)\right]\left(6-B\alpha^2h^2\right). \quad (31)$$

Resolving Eq. (31) for the steady state pressure gradient $q_0(z)$, one can get

$$q_0(z)=\frac{-96Q_0}{\left[f(t)h^4\left(6-B\alpha^2h^2\right)\right]}. \quad (32)$$

Substituting Eq. (32) in Eq. (30) and then simplifying, we get the expression for u_1 which is independent of $q_0(z)$ as below:

$$u_1=\frac{1}{64}\left[q_1(z)\,f(t)\right]h^2$$

$$\left[16\left\{1-(r/h)^2\right\}+B\alpha^2h^2\left\{3-4(r/h)^2+(r/h)^4\right\}\right]$$

$$+\frac{16(m-1)Q_0^3}{h^8\left(3-B\alpha^2h^2\right)}$$

$$\left[12\left\{1-(r/h)^4\right\}+B\alpha^2h^2\left\{16-9(r/h)^2-9(r/h)^4+2(r/h)^6\right\}\right] \quad (33)$$

Using Eq. (33), the expression for the first order approximation to volume flow rate can be obtained as given below:

$$Q_1=\int_0^h u_1\,r\,dr=\frac{\left[q_1(z)\,f(t)\right]\left(B\alpha^2h^2-6\right)h^4}{96}$$

$$+\frac{8(m-1)\left(9B\alpha^2h^2-8\right)Q_0^3}{h^6\left(3-B\alpha^2h^2\right)} \quad (34)$$

Resolving Eq. (34) for $q_1(z)$, we get

$$q_1(z)\,f(t)=-\frac{96Q_1}{\left(6-B\alpha^2h^2\right)h^4}$$

$$-\frac{256(m-1)\left(8-9B\alpha^2h^2\right)}{3\left(2-B\alpha^2h^2\right)}\left(\frac{Q_0^3}{h^{10}}\right). \quad (35)$$

Using Eqs. (35), (30) and (27) in Eq. (8) and then simplifying, one can get the expression for the velocity distribution as given below.

$$u=\frac{1}{64}\left[q(z)\,f(t)\right]h^2$$

$$\times\Big[16\left\{(r/h)^2-1\right\}+B\alpha^2h^2\left\{3-4(r/h)^2+(r/h)^4\right\}\Big]$$

$$+We^2\left(\frac{16(m-1)Q_0^3}{h^8\left(3-B\alpha^2h^2\right)}\right)$$

$$\times\Big[12\left\{(r/h)^4-1\right\}+B\alpha^2h^2\left\{16-9(r/h)^2-9(r/h)^4+2(r/h)^6\right\}\Big] \quad (36)$$

Applying Eqs. (32) and (35) in Eq. (9) yields the expression for the pressure gradient $q(z)=dp/dz$ as below:

$$q(z)\,f(t)=\frac{dp}{dz}\,f(t)=-\frac{96Q}{\left(6-B\alpha^2h^2\right)h^4}$$

$$-We^2\left(\frac{256(m-1)\left(8-9B\alpha^2h^2\right)}{3\left(2-B\alpha^2h^2\right)}\left(\frac{Q_0^3}{h^{10}}\right)\right) \quad (37)$$

The pressure drop $\Delta p\,f(t)$ in the stenosed arterial segment between the sections $z=0$ and $z=L$ is defined as

$$\Delta p\,f(t)=f(t)\int_0^L(-dp/dz)\,dz\,. \quad (38)$$

The longitudinal impedance to flow in the arterial segment of the artery between the sections $z=0$ and $z=L$ is defined and obtained as below:

$$\bar{\lambda}=\frac{\Delta p\;f(t)}{Q(t)}$$

$$=4\left\{\int_0^d F(z)\Big|_{R=1}dz+\int_d^{d+(3L_0/2)}F(z)\,dz+\int_{d+(3L_0/2)}^{L}F(z)\Big|_{R=1}dz\right\}, \quad (39)$$

where

$$F(z)=\frac{q(z)\,f(t)}{Q(t)}$$

$$=\frac{24}{\left(6-B\alpha^2h^2\right)h^4}+We^2\left(\frac{64(m-1)\left(8-9B\alpha^2h^2\right)}{3\left(2-B\alpha^2h^2\right)}\left(\frac{Q_0^2}{h^{10}}\right)\right) \quad (40)$$

Substituting Eq. (40) in Eq. (39) and then simplifying, we get the expression for longitudinal impedance to flow as

$$\bar{\lambda}=\left(L-\frac{3L_0}{2}\right)\left\{\frac{24}{\left(6-B\alpha^2\right)}+We^2\left(\frac{64(m-1)\left(8-9B\alpha^2\right)Q^2}{3\left(2-B\alpha^2\right)}\right)\right\}+\int_d^{d+(3L_0/2)}F(z)\,dz \quad (41)$$

The wall shear stress is defined as

$$\bar{\tau}_W=\tau\big|_{r=h}=\left[\left(\frac{\partial u}{\partial r}\right)+We^2\left(\frac{m-1}{2}\right)\left(\frac{\partial u}{\partial r}\right)^3\right]_{r=h}. \quad (42)$$

Eq. (36) yields the velocity gradient at the wall of the stenotic artery as

$$\left.\frac{\partial u}{\partial r}\right|_{r=h}=\frac{\left[q(z)\,f(t)\right]h\left(8-B\alpha^2h^2\right)}{16}+We^2\left(\frac{96Q_0^3(m-1)\left(8-7B\alpha^2h^2\right)}{h^9\left(3-B\alpha^2h^2\right)}\right) \quad (43)$$

Eq. (37) can be rewritten as

$$q(z)\,f(t)=-4Q\,F(z). \quad (44)$$

Substitution of Eq. (44) in Eq. (43) yields

$$\left.\frac{\partial u}{\partial r}\right|_{r=h}=4Q\,R(z), \quad (45)$$

where

$$R(z)=-\frac{F(z)h\left(8-B\alpha^2h^2\right)}{16}+\frac{24We^2Q^2(m-1)\left(8-7B\alpha^2h^2\right)}{h^9\left(3-B\alpha^2h^2\right)}. \quad (46)$$

Using Eq. (45) in Eq. (42), we get the expression for the wall shear stress as

$$\bar{\tau}_W=4Q\,R(z)+32We^2Q^3(m-1)R^3(z). \quad (47)$$

The maximum wall shear stress occurs at the throat of the stenosis $z=\sigma+1/n^{n/(n-1)}$ and is obtained as below:

$$\bar{\tau}_S=\bar{\tau}_W\big|_{h=1-\delta}=4QJ+32We^2Q^3(m-1)J^3, \quad (48)$$

where

$$J=-\frac{K(1-\delta)\left[8-B\alpha^2(1-\delta)^2\right]}{16}+24\left(\frac{We^2\,Q^2\,(m-1)\left[8-7B\alpha^2(1-\delta)^2\right]}{(1-\delta)^9\left[3-B\alpha^2(1-\delta)^2\right]}\right), \quad (49)$$

and

$$K=F(z)\big|_{h=1-\delta}=\frac{24}{(1-\delta)^4\left[6-B\alpha^2(1-\delta)^2\right]}+64\,We^2\left\{\frac{Q^2\,(m-1)\left[8-9B\alpha^2(1-\delta)^2\right]}{3(1-\delta)^{10}\left[2-B\alpha^2(1-\delta)^2\right]}\right\} \quad (50)$$

We introduce the following normalization variables to the longitudinal impedance to flow, wall shear stress and shear stress at the throat of the stenosis:

$$\lambda=\bar{\lambda}/\lambda_0;\ \tau_W=\bar{\tau}_W/\tau_0;\ \tau_S=\bar{\tau}_S/\tau_0, \quad (51)$$

where $\lambda_0=3L$ and $\tau_0=4Q$ are the resistance to flow and wall shear stress in the normal artery (without constriction and tapering) respectively [30]. Applying Eqs. (41), (47) and (48) in Eq. (51), the expression for the normalized flow quantities such as longitudinal impedance to flow, wall shear stress and shear stress at the throat of the stenosis are derived as below respectively:

$$\lambda=\frac{1}{3}\left[\left(1-\frac{3L_0}{2L}\right)\left\{\frac{24}{\left(6-B\alpha^2\right)}+We^2\left(\frac{64Q^2(m-1)\left(8-9B\alpha^2\right)}{3\left(2-B\alpha^2\right)}\right)\right\}\right]+\frac{1}{3L}\int_d^{d+(3L_0/2)}F(z)\,dz \quad (52)$$

$$\tau_W=R(z)+8(m-1)We^2Q^2R^3(z), \quad (53)$$

$$\tau_S=J+8(m-1)We^2Q^2J^3. \quad (54)$$

when $\alpha^2=0$, the expressions obtained for the flow quantities reduce to the flow quantities of steady flow and these reduced expressions of the flow quantities are in very good agreement with the expressions obtained for the corresponding flow quantities by Akbar and Nadeem [18].

4. Numerical Simulation of Results and discussion

The main objective of the of this mathematical analysis is to investigate the effects of asymmetric nature of stenosis, non-Newtonian nature of blood on the physiologically important flow quantities such as velocity distribution, wall shear stress and longitudinal impedance to flow of blood, when it flows through tapered narrow artery with mild asymmetric stenosis, treating blood as Carreau fluid model. The range of parameters which are used to analyze and validate the flow are listed below [18, 19]:

Power law index: 2 – 6; Maximum depth of the stenosis δ: 0 – 0.15; stenosis shape parameter n: 2 – 7; Weissenberg numer We: 0.2 – 0.5: Flow rate Q: 0.2 – 0.5; 0.3 – 0.5;

Pulsatile Reynolds number α: 0.2 – 0.7; Angle of tapering ψ: - 0.1° – 0.1°; Amplitude of time dependent part of pressure gradient A: 0.2 – 0.5.

4.1 Velocity distribution

Figure 2 delineates the velocity distribution for different values of n and δ with $Q = We = 0.3$, $t = 45^{o}$, $\alpha = 0.2$, $z = 0.5$, $\psi = -0.1°$ and $A = 0.2$. One can notice the parabolic velocity profile with maximum velocity at the centre of the conduit which is well known for laminar flow of viscous incompressible fluids. It is observed that the velocity of blood decreases considerably with the increase of maximum depth of the stenosis δ, whereas, it increases marginally with the increase of the stenosis shape parameter n. Velocity distribution for different values of power law index m and at different locations of the stenosis in the axial direction with $Q = We = 0.3$, $t = 60°$, $\alpha = 0.2$, $z = 0.5$, $\psi = 0°$, $A = 0.2$, $\delta = 0.05$ and $n = 6$ is sketched in Figure 3.It is noted that at any cross-section of the stenosis, the velocity of blood increases considerably with the increase of the power law index m. It is also found that the blood velocity decreases marginally with the increase of the constriction of the flow region, i.e the fluid velocity decreases when the cross-sectional area of the fluid flow decreases.

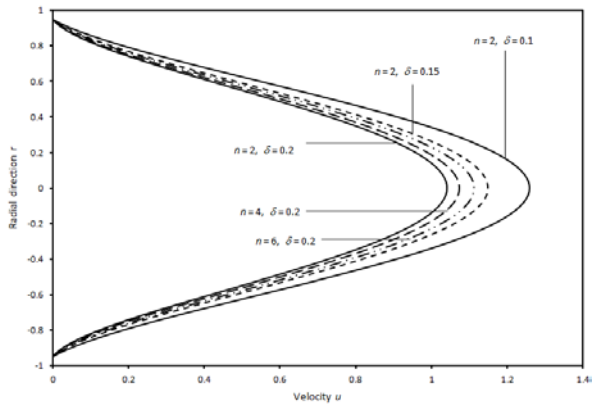

Figure 2. Velocity distribution for different values of n and δ with $Q = We = 0.3$, $t = 45^{o}$, $\alpha = 0.2$, $z = 0.5$, $\psi = -0.1°$ and $A = 0.2$.

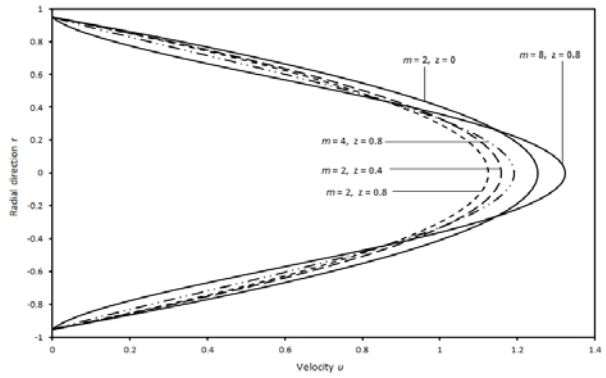

Figure 3. Velocity distribution for different values of m and z with $Q = We = 0.3$, $t = 60°$, $\alpha = 0.2$, $z = 0.5$, $\psi = 0°$, $A = 0.2$, $\delta = 0.05$, $n = 6$.

4.2 Wall shear stress

The variation of wall shear stress with axial distance for different values of stenosis shape parameter n, pulsatile Reynolds number α and maximum depth of the stenosis δ with $Q = 0.18$, $We = 0.5$, $t = \psi = 0°$, $A = 0.2$ and $m = 2$ is shown in Figure 4. It is seen that the wall shear stress increases with the increase of the axial distance from $z = 0$ to the point where the stenosis depth is maximum and then it decreases from that point to $z = 1$. (The maximum stenosis depth occurs exactly at $z = 0.5$ when the stenosis is axi-symmetric ($n = 2$) and this point moves towards right side when the stenosis shape parameter n increases from 2 to 8).
One can note that for a given value of the pulsatile Reynolds number α, the wall shear stress decreases significantly with the increase of the amplitude A of the of the pulsatile pressure gradient and stenosis shape parameter n, whereas, it increases very significantly with the increase of the pulsatile Reynolds number α when all the other parameters are held constant. When $\alpha = 0$, the present study reduces to steady flow case and in such case the plot of the wall shear stress in Figure 4 is in good agreement with the corresponding plot in Figure 9 of Akbar and Nadeem. Figure 5 illustrates the variation of wall shear stress with the maximum depth of the stenosis δ for different values of flow rate Q and Weissenberg number We with $n = m = 2$, $A = \alpha = 0.2$, $t = 45°$, $z = 0.5$ and $\psi = 0°$. It is clear that the wall shear stress increases slightly nonlinear with the increase of the maximum depth of the stenosis δ. It is found that the wall shear stress decreases marginally with the increase of the Weissenberg number We and flow rate Q.

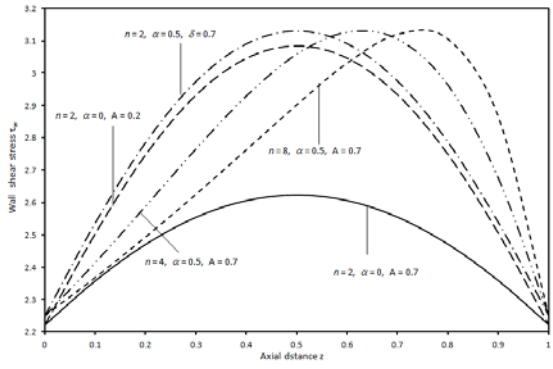

Figure 4 Variation of wall shear stress with axial distance for different values of n, a and d with $\psi = 0$, Q = We = 0.3, t = 0^{o}, A = 0.2 and $m = 2$.

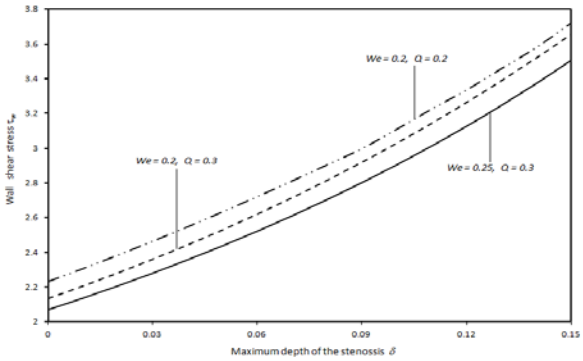

Figure 5. Variation of wall shear stress with maximum depth of the stenosis for different values of We and Q with $n = m = 2$, $A = \alpha = 0.2$, $t = 45°$, $z = 0.5$ and $\psi = 0$.

4.3 Longitudinal impedance to flow

Figure 6 depicts the variation of longitudinal impedance to flow with the maximum depth of the stenosis for different values of Q, A, α and n with $We = 0.5$, $m = 2$, $t = 45°$, and $\psi = 0°$. It is found that the longitudinal impedance to flow increases linearly with the increase of the maximum depth of the stenosis from 0 to 0.75 and then it increases rapidly with the increase of the maximum depth of the stenosis from 0.75 to 0.15. For a given set of values of the parameters α and Q, the longitudinal impedance to flow decreases marginally with the increase of the stenosis shape parameter n and amplitude of the unsteady part of the pressure gradient A. One can also note that the longitudinal impedance to flow decreases significantly with the increase of the flow rate and decreases considerably with the increase of the pulsatile Reynolds number of the blood flow when all the other parameters kept fixed.

The variation of longitudinal impedance to flow with maximum depth of the stenosis for different values of We and m with $Q = 0.3$, $A = \alpha = 0.2$, $n = 2$, $\psi = 0.1°$ and $t = 60°$ is illustrated in Figure 7. It is also seen that the longitudinal impedance to flow decreases significantly with the increase of the power law index m and Weissenberg number We when all the other parameters are treated as invariables.

4.4 Quantification of physical quantities

Longitudinal impedance to flow and wall shear stress are some of the important flow quantities which are used in the clinical analysis of blood flow. Accurate predictions of these flow quantities are useful in the investigation of blood flow on the endothelial cells [32]. Estimates of the percentage of increase in wall shear stress different cross sections of the artery and for different maximum depths of stenosis with $n = 4$, $Q = We = 0.3$, $t = 315°$, $A = \alpha = 0.2$, $m = 2$, $\psi = 0°$. It is noted that the estimates of the percentage of increase in the wall shear stress increases significantly with the increase of the axial distance from $z = 0.1$ to $z = 0.7$ (since $n = 4$ corresponds to asymmetric shape of stenosis) and then it decreases with the increase of the axial distance from $z = 0.7$ to $z = 0$ .9. It is also observed that the estimates of the percentage of increase in the wall shear stress increases rapidly with the increase of the maximum depth of the stenosis when all the other parameters held constant. Table 2 computes the estimates of the percentage of increase in the wall shear stress for different angles of tapering and for different values of stenosis shape parameter with $Q = We = 0.3$, $t = 315$, $A = \alpha = 0.2$, $m = 2$ and $\psi = 0°$. It is found that estimates of the percentage of increase in the wall shear stress increase slightly with the increase of angle of tapering ψ and stenosis shape parameter n.

The estimates of the percentage of increase in the longitudinal impedance to flow for different values of δ and m with $Q = We = 0.3$, $t = 60°$, $A = \alpha = 0.2$ and $m = n = 4$ are computed in Table 3. It is recorded that the estimates of the percentage of increase in the longitudinal impedance to flow decreases slightly with the increase of the angle of tapering and increases rapidly with the increase of the maximum depth of the stenosis δ. for different values of δ and m with $Q = We = 0.3$, $t = 60°$, $A = \alpha = 0.2$, $\psi = 0°$ and $m = n = 4$. Table 4 computes the estimates of the percentage of increase in the longitudinal impedance to flow for different values of δ and m with $Q = We = 0.3$, $t = 60°$, $A = \alpha = 0.2$, $m = n = 4$. It is observed that the estimates of the longitudinal impedance to flow decreases marginally with the increase of the stenosis shape parameter n.

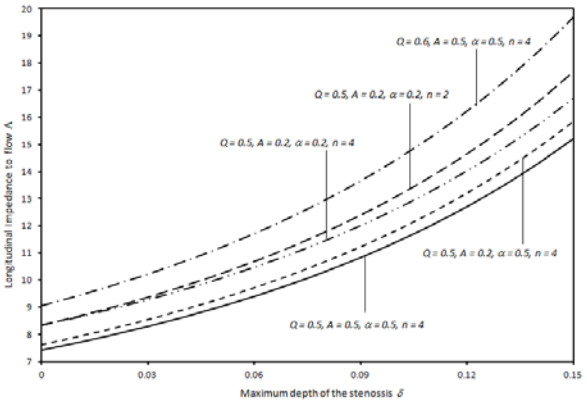

Figure 6. Variation of longitudinal impedance to flow with maximum depth of the stenosis for different values of Q, A, α and n with $We = 0.5$, $m = 2$, $t = 45°$ and $\psi = 0°$.

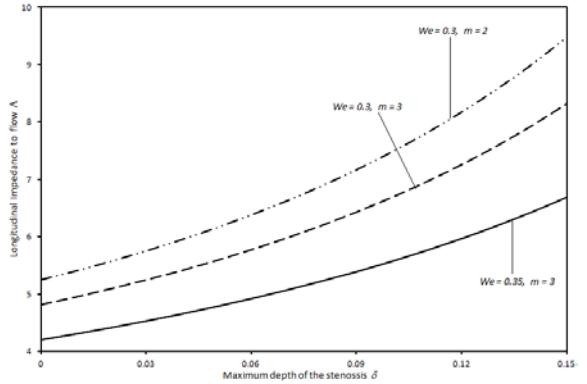

Figure 7. Variation of longitudinal impedance to flow with the maximum depth of the stenosis for different values of We, m and ψ with $Q = 0.3$, $A = \alpha = 0.2$, $n = 2$, $\psi = 0.1°$ and $t = 60°$.

Table 1. Estimates of the percentage of increase in wall shear stress different cross sections of the artery and for different maximum depths of stenosis with $n = 4$, $Q = We = 0.3$, $t = 315°$, $A = \alpha = 0.2$, $m = 2$, $\psi = 0°$.

δ	z = 0.1	z = 0.3	z = 0.5	z= 0.7	z = 0.9
0.025	1.43	4.34	7.13	8..64	5.38
0.05	2.88	8.89	14.81	18.06	11.07
0.075	4.35	13.65	22.98	28.16	17.07
0.1	5.85	18.6	31.58	38.72	23.35
0.125	7.37	23.74	40.42	49.3	29.87
0.15	8.92	29.02	49.2	59.08	36.56

Table 2. Estimates of the percentage of increase in the wall shear stress for different angles of tapering and for different values of stenosis shape parameter with $Q = We = 0.3$, $t = 315$, $A = \alpha = 0.2$, $m = 2$ and $\psi = 0°$.

ψ	n = 2	n = 3	n = 4	n = 5	n = 6
-0.05°	0.120	0.121	0.126	0.128	0.127
-0.1°	0.243	0.245	0.249	0.253	0.256
0.05°	-0.120	-0.121	-0.123	-0.125	-0.130
0.1°	-0.240	-0.245	-0.249	-0.253	-0.256

Table 3. Estimates of the percentage of increase in the longitudinal impedance to flow for different values of δ and m with $Q = We = 0.3$, $t = 60°$, $A = \alpha = 0.2$ and $m = n = 4$.

δ \ ψ	- 0.05°	- 0.1°	0°	0.05°	0.1°
0.025	7.71	7.69	7.68	7.67	7.66
0.05	16.91	16.88	16.85	16.82	16.79
0.075	28	27.94	27.89	27.84	27.79
0.1	41.5	41.42	41.34	41.26	41.19
0.125	58.13	58.02	57.9	57.79	57.68
0.15	78.88	78.72	78.56	78.4	78.24

Table 4. Estimates of the percentage of increase in the longitudinal impedance to flow for different values of δ and m with $Q = We = 0.3$, $t = 60°$, $A = \alpha = 0.2$, $m = 4$ and $\psi = 0°$.

δ \ n	2	3	4	5	6
0.025	6.4	6.23	6.08	5.95	5.85
0.05	13.81	13.42	13.09	12.81	12.57
0.075	22.44	21.8	21.24	20.78	20.38
0.1	32.61	31.65	30.82	30.12	29.53
0.125	44.71	43.36	42.17	41.19	40.36
0.15	59.27	57.43	55.8	54.45	53.32

4.5 Some clinical applications

To provide some physiological applications to the present study, the clinical data (arteries of different types, their diameters, steady and pulsatile pressure gradients values) used by Sankar et al. [11] are given in Table 5. The estimates of the mean velocity $\left(10^{-2}\,\mathrm{m\,s^{-1}}\right)$ of blood in steady and pulsatile flow of blood through arteries of different radii for different values of angle of tapering ψ with $t = 45°$, $n = 4$, $We = Q = 0.3$, $z = 0.5$, $m = 2$, and $\delta = 0.1$ are computed in Table 6. It is noted that the mean velocity of blood decreases considerably with the increase of the artery radius (except in arteriole) and angle of tapering. One can observe that the mean velocity of blood is considerably higher in pulsatile flow of blood than in the steady flow of blood. It is also found that the mean velocity of blood is highest in coronary arteries and is lowest in arterioles. Table 7 computes the mean velocity $\left(10^{-2}\,\mathrm{m\,s^{-1}}\right)$ of blood in steady and pulsatile flows for the different values of δ in arteries with different radii with $t = 60°$, $We = Q = 0.3$, $z = 0.5$, $m = 2$, $n = 4$ and $\psi = 0.1°$. It is observed that the mean velocity of blood decreases considerably with the increase of the maximum depth of the stenosis.

Table 5 Physiological data for arteries of different radii.

Artery type	Diameter $\left(\mathrm{x}\ 10^{-2}\mathrm{m}\right)$	A_0 $\left(\mathrm{x}\ 10\,\mathrm{Kg\ m^{-2}\,s^{-1}}\right)$	A_1 $\left(\mathrm{x}\ 10\,\mathrm{Kg\ m^{-2}\,s^{-1}}\right)$
Aorta	2.0	7.3	1.46
Femoral	1.0	32.0	6.4
Carotid	0.8	50.0	10.0
Coronary	0.3	698.65	139.74
Arteriole	0.016	2000.0	400

Table 6 The estimates of the mean velocity $\left(10^{-2}\,\mathrm{m\,s^{-1}}\right)$ of blood in steady and pulsatile flows for blood flow through arteries of different radii and for different values of ψ with $t = 45°$, $We = Q = 0.3$, $z = 0.2$, $m = 2$, $n = 4$, $\delta = 0.1$.

Artery Type	Steady flow			Pulsatile flow		
	Angle of tapering ψ			Angle of tapering ψ		
	- 0.1°	0°	0.1°	- 0.1°	0°	0.1°
Aorta	44.89	40.33	36.81	51.15	47.34	43.12
Femoral	50.75	45.29	41.32	56.35	52.17	48.28
Carotid	52.16	48.55	43.63	57.12	53.34	50.15
Coronary	90.44	88.58	84.43	97.51	93.21	90.23
Arteriole	0.77	0.65	0.51	0.87	0.77	0.65

Table 7. Estimates of mean velocity $\left(10^{-2}\,\mathrm{m\,s^{-1}}\right)$ of blood in steady and pulsatile flows and the difference between them for the different values of δ in arteries with different radii with $t = 60°$, $z = 0.5$, $We = Q = 0.3$, $m = 2$, $n = 4$ and $\psi = 0.1°$.

Artery Type	Steady flow			Pulsatile flow		
	Maximum depth of stenosis δ			Maximum depth of stenosis δ		
	0.05	0.1	0.15	0.05	0.1	0.15
Aorta	47.52	44.62	41.27	53.85	50.25	46.63
Femoral	53.96	49.95	47.65	58.47	54.68	51.94
Carotid	55.41	50.36	48.13	60.18	55.72	52.55
Coronary	97.47	94.54	90.48	99.14	97.37	94.16
Arteriole	0.82	0.73	0.65	0.94	0.82	0.71

5. Conclusions

The pulsatile flow of blood in a tapered arterial segment with asymmetric stenosis is analyzed mathematically, treating blood as non-Newtonian Carreau fluid. The main findings of this mathematical analysis are summarized below:

- The velocity of blood increases marginally with the increase of the power law index m and stenosis shape parameter n and it decreases considerably with the increase of the maximum depth of the stenosis n.

- The wall shear stress and longitudinal impedance to flow increases significantly with the increase of the maximum depth of the stenosis δ and they increase marginally with the increase of the pulsatile Reynolds number α.
- The wall shear stress and longitudinal impedance to flow decreases with the increase stenosis shape parameter *n*, amplitude of the pulsatile pressure gradient *A*, flow rate *Q*, power law index *m* and Weissenberg number *We*.
- The estimates of the percentage of increase in the wall shear stress and longitudinal impedance to flow increase slightly with the increase of the angle tapering ψ and these estimates increase significantly with the increase of the maximum depth of the stenosis δ.
- The estimates of the percentage of increase in the wall shear stress and longitudinal impedance to flow decrease marginally with the increase of the stenosis shape parameter *n*.
- The mean velocity of blood decreases considerably with the increase of the artery radius (except in arteriole), maximum depth of the stenosis δ and angle of tapering ψ.
- The mean velocity of blood is considerably higher in pulsatile flow of blood than in the steady flow of blood.

From the aforementioned results, one can note that there is significant difference between the corresponding estimates of mean velocities of blood in steady and pulsatile flows and which cannot be neglected. It is hoped that the results of the present study can be used to predict physiologically important flow measurements in the normal and abnormal states and to recommend appropriate method of therapy to clear the constriction in the artery. Thus, it is concluded that the present study may be considered as an improvement in the studies of pulsatile blood flow through tapered narrow artery with mild asymmetric stenosis.

References

[1] D. F. Young, "Fluid mechanics of arterial stenosis," *J. Biomech. Engng (Trans. ASME)* vol. 101, pp. 157 – 175, 1979.

[2] F. T. Smith, "The separation of flow through a severely constricted symmetric tube," *J. Fluid Mech.,* vol. 90, pp. 725 – 754, 1979.

[3] J. N. Kapur, "Mathematical models in Biology and Medicine", Affiliated East -West Press Pvt Ltd, New Delhi, India, pp. 368 – 369, 1992.

[4] K. W. Lee, X. Y. Xu, "Modeling of flow and wall behavior in a mildly stenosed tube", *Med. Engng. Phys.* Vol. 24, pp. pp. 575 – 586, 2002.

[5] Kh. S. Mekheimer, M. A. El Kot, "Mathematical modeling of unsteady flow of Sisko fluid through an anisotropically tapered elastic arteries with time-variant overlapping stenosis," *App. Math. Model.,* vol. 36, pp. 5393 – 5407, 2012.

[6] P. R. Johnston, D. Kilpatrick, "Mathematical modeling of flow through irregular arterial stenoses," *J. Biomech.* vol. 24, pp. 1069 – 1077, 1991.

[7] P. R. Johnston, D. Kilpatrick, "Mathematical modeling of flow through irregular arterial stenoses," *J. Biomech.*, vol. 24, pp. 1069 – 1077, 1991.

[8] S. Nadeem and S. Ijaz, "Mechanics of biological blood flow analysis through curved artery with stenosis," *J. Mech. Med. Biol.*, **16**, 1650024, 2016, DOI: http://dx.doi.org/10.1142/S021951941650024X.

[9] P. Chaturani, R. Ponnalagar Samy, "A study of non Newtonian aspects of blood flow through stenosed arteries and its applications in arterial diseases," *Biorheology*, vol. 22, pp. 521–31, 1985.

[10] S. Chakravarty, P. K. Mandal, A. Mandal, "Mathematical model of pulsatile blood flow in a distensible aortic bifurcation subject to body acceleration," *Int. J. Engg. Sci.*, vol. 38, pp. 215 – 238, 2000.

[11] R.K. Dash, G. Jayaraman, K.N. Metha, "Estimation of increased flow resistance in a narrow catheterized artery – A theoretical model'" *J. Biomech.* vol. 29, pp. 917–930, 1996.

[12] C. Tu, M. Deville, "Pulsatile flow of non-Newtonian fluids through arterial stenosis", *J. Biomech.*, vol. 29 pp. 899 – 908, 1996.

[13] Md. A. Ikbal, S. Chakravarty, K.L. Kelvin Wong, J. Mazumdar, P.K. Mandal, "Unsteady response of non-Newtonian blood flow through a stenosed artery in magnetic field," *J. Comput. Appl. Math.*, vol. 230 pp. 243-259, 2009.

[14] Y. I. Cho, K. R. Kensey, "Effects of the non-Newtonian viscosity of blood on hemodynamics of diseased arterial flows," *Adv. BioEngng.*, vol. 15 pp. 147 – 148, 1989.

[15] B. M. Jonhston, P.R. Johmston, S. Corney, D. Kilpatrick, "Non-Newtonian blood flow in human right coronary arteries steady state simulations," *J. Biomech.*, vol. 37 pp. 709 – 720, 2004.

[16] W. Y. Chang, Y. Ding, J. Y. Tu, "Modeling of non-Newtonian blood flow through a stenosed artery incorporating fluid structure interaction," *Australia and New Zealand J. Appl. Math.*, vol. 47, pp. 507 – 523, 2007.

[17] N. S. Akbar, "Heat and mass transfer on Carreau fluid model for blood flow through a tapered artery with a stenosis," *Int. J. Biomath,*. vol. 7, 145004, 2014.

[18] N. S. Akbar, S. Nadeem, "Carreau fluid model for blood flow through a tapered artery with a stenosis," *Ain Shams Engng. J.,* vol. 5, pp. 1307 – 1316, 2014.

[19] D. S. Sankar, "Perturbation analysis for pulsatile flow of Carreau fluid through tapered stenotic arteries," *Int. J. Biomath.,* vol. 9, 1650063, 2016.